

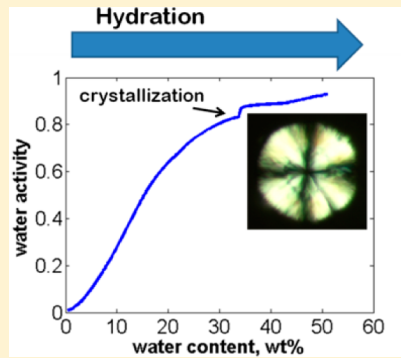
Hydration of Hyaluronan: Effects on Structural and Thermodynamic Properties

Cathrine Albèr, Johan Engblom, Peter Falkman, and Vitaly Kocherbitov*

Biomedical Science, Faculty of Health and Society and Biofilms – Research Center for Biointerfaces, Malmö University, SE-205 06 Malmö, Sweden

 Supporting Information

ABSTRACT: Hyaluronan (HA) is a frequently occurring biopolymer with a large variety of functions in nature. During the past 60 years, there have been numerous reports on structural and dynamic behavior of HA in water. Nevertheless, studies covering a wider concentration range are still lacking. In this work, we use isothermal scanning sorption calorimetry for the first time to investigate hydration-induced transitions in HA (sodium hyaluronate, 17 kDa). From this method, we obtain the sorption isotherm and the enthalpy and the entropy of hydration. Thermotropic events are evaluated by differential scanning calorimetry (DSC), and structure analysis is performed with X-ray scattering (SWAXS) and light and scanning electron microscopy. During isothermal hydration, HA exhibits a glass transition, followed by crystallization and subsequent dissolution of HA crystals and formation of a one-phase solution. Structural analysis reveals that the crystal may be indexed on an orthorhombic unit cell with space group $P2_12_12_1$. Crystallization of HA was found to occur either through endothermic or exothermic processes, depending on the temperature and water content. We propose a mechanism of crystallization that explains this phenomenon based on the interplay between the hydrophobic effect and strengthening of hydrogen bonds during formation of crystals. The combined results were used to construct a binary phase diagram for the HA–water system.



1. INTRODUCTION

Hyaluronic acid, also referred to as hyaluronan (HA), is an unbranched anionic polysaccharide composed of repeating units of *N*-acetylglucosamine and glucuronic acid connected by β -linkages (Figure 1).^{1,2} HA is a major component of the

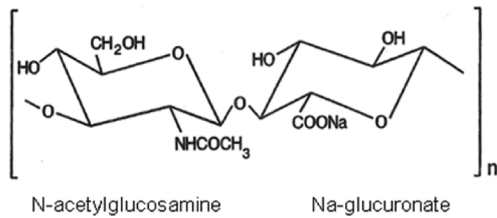


Figure 1. Repeating disaccharide unit of HA sodium salt.

extracellular matrix of vertebrates, where it is involved in maintaining osmotic balance and reducing friction in liquid connective tissues such as the joint synovial fluid and eye vitreous. The concentration of HA in the synovial fluid has been determined to be 0.14–0.36 wt % with a molecular weight of several million Dalton.^{2,3} At these concentrations and molecular masses, the HA chains overlap and entangle, which results in a flexible matrix at physiological conditions. Owing to its viscoelasticity, the ability to interact with water, as well as its biocompatibility, HA has gained special interest in several medical and cosmetic applications. For example, HA has been

used as a substitute for vitreous fluid in ophthalmic surgery, for cutaneous wound healing, in injectable dermal fillers, and as moisturizing agents in skin care products.^{4–7}

The variety in biological functions of HA suggests the existence of a correspondingly large collection of conformations. During the past 60 years, numerous studies have been reported on the structural and dynamic behavior of HA at various experimental conditions; however, studies performed over a wider concentration range are still lacking. In dilute solutions at physiological conditions, HA chains are believed to obtain a stiffened random coil configuration that occupies a large hydrodynamic volume. Its local stiffness, resulting in a persistence length of about 5–7 nm, has been attributed to electrostatic repulsion among carboxylate groups in combination with the hydrogen bonds between the adjacent monosaccharide units and/or with hydrogen bonds with the surrounding water molecules.^{3,8} Furthermore, it was shown that the hydrogen-bonded secondary structure shows arrays of contiguous –CH groups, giving a hydrophobic character to some part of the polymer.^{9,10} It was suggested that these hydrophobic domains could mediate self-aggregation and be the basis of interactions with lipid membranes and proteins in vivo. X-ray studies have indicated that semihydrated fibers and

Received: November 18, 2014

Revised: February 20, 2015

Published: February 26, 2015



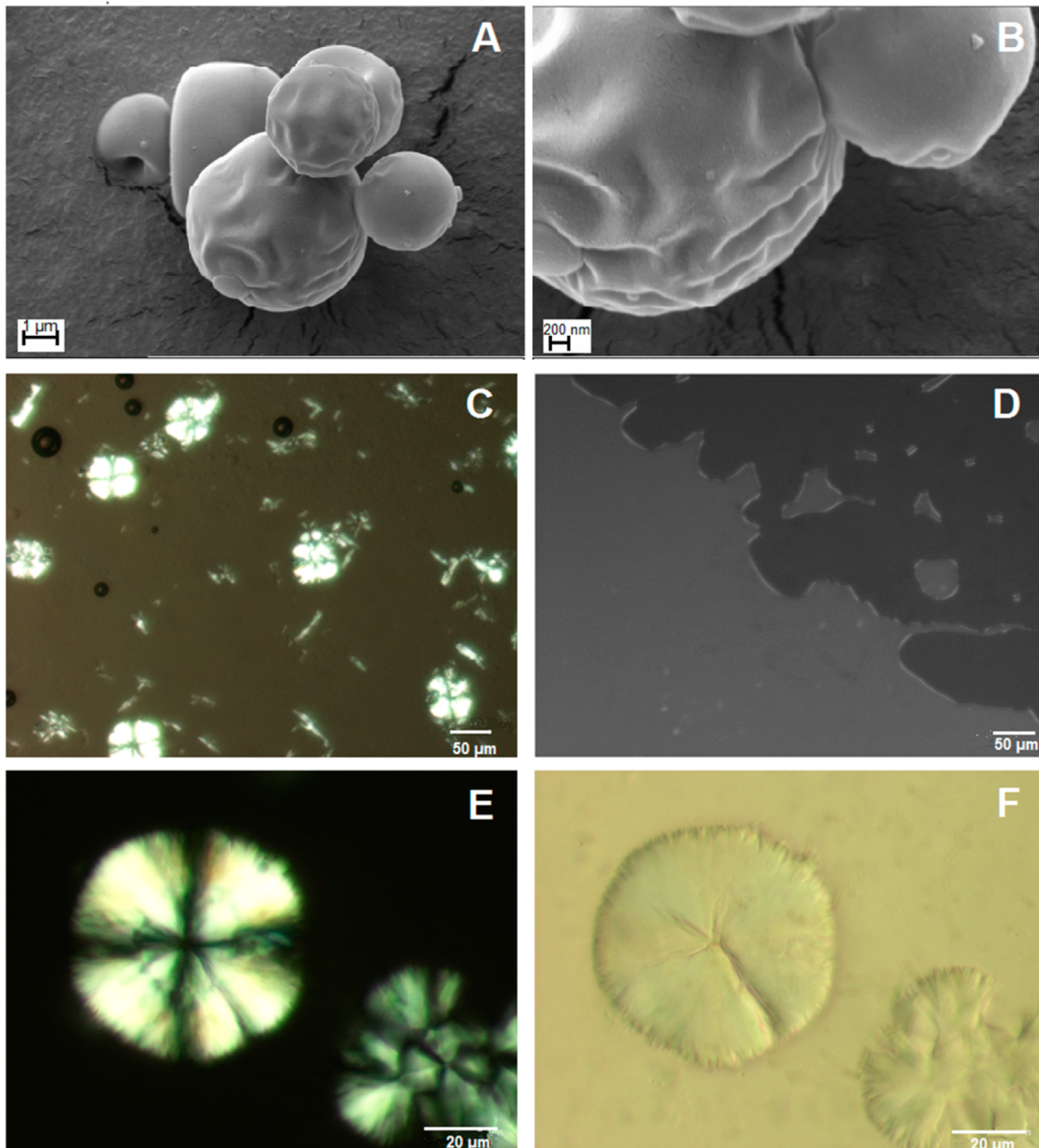


Figure 2. Micrographs of HA samples obtained with SEM (A,B) and polarized light microscopy (C–F). Dry HA particles in vacuum with two different magnifications are shown in (A) and (B). (C) and (E) show birefringent crystals in a HA–water mixture with 60 wt % HA, while no optical birefringence was observed in a sample with 40 wt % HA (D). For comparison, (F) shows the same samples as that in (E) but without cross-polarized filters.

films of HA can adopt two-, three- and four-fold helical conformations as well as double-helix structure with hexagonal, orthorhombic, or tetragonal unit cells.^{11–14} It was also shown that formation of ordered HA arrangements is highly dependent on the experimental conditions such as relative humidity, temperature, pH, and type of counterion.¹²

In the present work, we aim to investigate the effect of hydration and temperature on HA (sodium hyaluronate, 17 kDa) at concentrations ranging from the dry to dilute state. Data obtained from a combination of several techniques such as isothermal sorption calorimetry, small and wide-angle X-ray scattering (SWAXS), and differential scanning calorimetry (DSC) are used to present a binary phase diagram of the HA–water system.

2. MATERIAL AND METHODS

Chemicals. HA, (sodium hyaluronate, MW 17 kDa) was kindly provided by Q-med AB (Uppsala, Sweden) and was used without further purification. Before any hydration procedure, HA samples were dried in vacuum in contact with 3 Å molecular sieves for 24 h at room temperature. Samples for DSC and SWAXS studies were prepared either by adding water directly to dry HA or by equilibrating dry HA at a controlled relative humidity (25 °C) using the following saturated salt solutions: K₂SO₄ (97.30% RH), KNO₃ (93.58% RH), KCl (84.34% RH), KBr (80.89% RH), NaCl (75.29% RH), SrCl₂ (70.85% RH), Mg(NO₃)₂ (52.89% RH), MgCl₂ (32.78% RH), and LiCl (11.30% RH).¹⁵

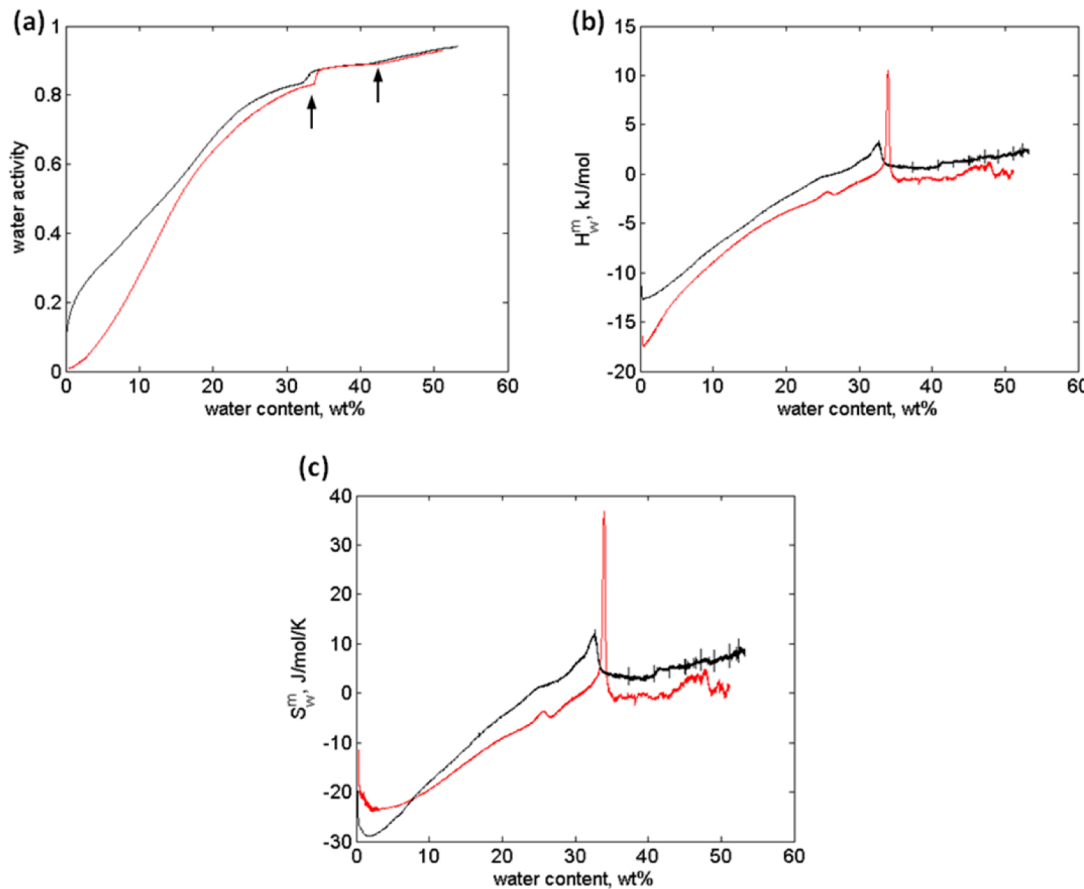


Figure 3. Sorption isotherms (a) and partial molar enthalpy (b) and entropy (c) of mixing of water as a function of water content of untreated HA (red curves) and of the same material recrystallized prior to hydration (black curves). Arrows indicate the points of crystallization and the point where the two-phase region ends. Experiments were performed at 25 °C.

Scanning Electron Microscopy. The appearance of dry HA particles was examined with a scanning electron microscope (Zeiss EVO LS10) equipped with a LaB6 filament. Dry HA particles were sputter-coated with gold using an Agar automatic sputter coater at 30 mA, 0.08 mbar of pressure, and with a sputtering time of 40 or 60 s prior to analysis. The particles were then imaged in high-vacuum mode using a secondary electron detector, at a 10 kV accelerating voltage, 50 pA probe current, and 9 mm working distance.

Polarized Light Microscopy. Different compositions of HA–water mixtures were studied with a light microscope equipped with cross-polarizing filters (Nikon Optiphot, Nikon Corporation, Tokyo, Japan) at room temperature (25 °C).

Isothermal Sorption Calorimetry. To investigate the hydration-driven transitions in HA, we used isothermal sorption calorimetry, which simultaneously gives the sorption isotherm and the partial molar enthalpy and entropy of mixing of water. Sorption calorimetric experiments were conducted at 25, 40, and 50 °C in a two-chamber sorption calorimetric cell inserted in a double-twin microcalorimeter.¹⁶ Vacuum-dried HA was loaded into the upper (sorption) chamber under a dry atmosphere in a glovebox. The experiment was initiated by injecting pure water into the lower (vaporization) chamber. During the experiment, water evaporated from the lower vaporization chamber and was then absorbed by the sample in the upper sorption chamber. The thermal powers released in the two chambers were monitored simultaneously. The activity of water, a_w , in the sorption experiment was calculated from the

thermal power of the vaporization of water in the lower chamber, as described by Kocherbitov.¹⁷ From the same experiment, the partial molar enthalpy of mixing of water, H_w^m , (hydration enthalpy) was calculated using the following equation

$$H_w^m = H_w^{\text{vap}} + H_w^{\text{vap}} \frac{P^{\text{sorp}}}{P^{\text{vap}}} \quad (1)$$

where P^{vap} and P^{sorp} are thermal powers registered in the vaporization and sorption chambers, respectively, and H_w^{vap} is the molar enthalpy of evaporation of pure water. Combining the water activity and the enthalpy data, one can calculate the partial molar entropy of mixing of water S_w^m

$$S_w^m = \frac{H_w^m}{T} - R \ln a_w \quad (2)$$

SWAXS. SAXS measurements were performed at the MAX IV Laboratory (Lund, Sweden) at the Swedish–Danish beamline Cassiopeia (I911-SAXS).¹⁸ The wavelength of the beam was 0.91 Å, and the sample to detector distance was 1327 mm. The software Fit2d (Hammersley, 1997) and CHEKCELL (INPG, France) and programs written in Matlab (Mathworks U.S.A.) were used for data evaluation. WAXS measurements were conducted with a SWAXS compact Kratky camera with line collimation ($\lambda(\text{Cu } K_\alpha) = 1.542 \text{ \AA}$) HECUS X-ray systems (Graz, Austria). Background subtraction (empty solid sample holder or capillary filled with water) was performed using programs written in Matlab.

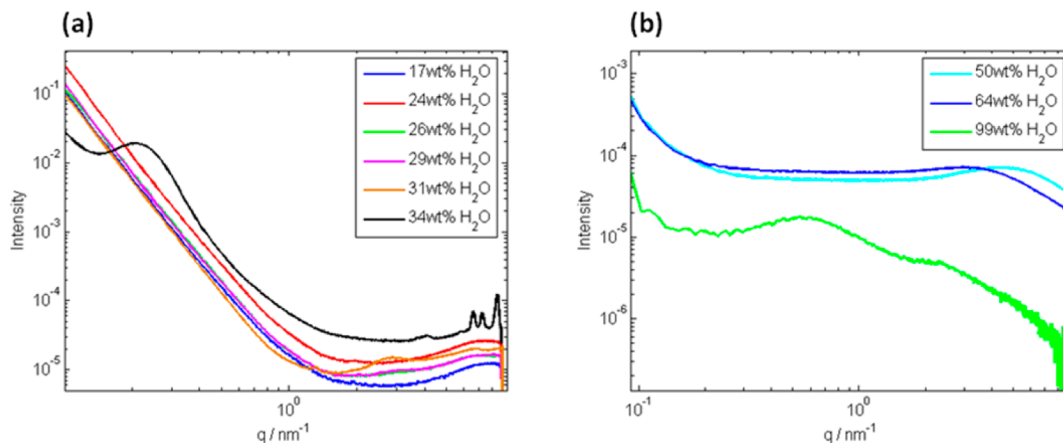


Figure 4. SAXS spectra (intensity versus scattering vector, q) of hydrated HA samples in the concentrated regime (a) and dilute regime (b). The legends show the water content in wt %.

DSC. HA samples of different hydration levels were examined by DSC (DSC 1, Mettler Toledo) using hermetically sealed aluminum pans ($40\ \mu\text{L}$, Mettler Toledo). Samples were cooled from room temperature to $-80\ ^\circ\text{C}$, held at this temperature for 10 min, and subsequently heated to $95\text{--}120\ ^\circ\text{C}$ at a scanning rate of $5\ ^\circ\text{C}/\text{min}$. In addition, several lower scan rates (1, 0.5, and $0.2\ ^\circ\text{C}/\text{min}$) were used for samples with high water content in order to extrapolate the endset of melting of ice to zero scan rate. Indium was used as a calibrant, and an empty sealed aluminum pan was used as a reference.

3. RESULT AND DISCUSSION

Microscopy. Figure 2 shows a selection of micrographs of HA samples obtained with SEM (A,B) and polarized light microscopy (C–F). SEM micrographs of dry HA particles in vacuum reveal a rather smooth particle surface, although wrinkles are observed at larger magnification (Figure 2A,B). Clusters of dry spherical HA particles were observed with a particle size distribution between ~ 0.2 and $15\ \mu\text{m}$. Different HA–water mixtures were analyzed with cross-polarized light microscopy. Birefringent crystals were, for example, observed in samples with 60 wt % HA (C), while in a less concentrated sample with 40 wt % HA (D), the optical birefringence disappeared, which suggests a one-phase solution. A magnification of the crystals observed with 60 wt % HA in water is shown with (E) and without (F) cross-polarized filters.

Isothermal Sorption Calorimetry. Water vapor sorption isotherms of native and cross-linked HA have previously been determined gravimetrically.^{19–22} However, there is a need for sorption isotherms based on scanning methods that allow for high-resolution continuous scanning of the sample in a broad range of relative vapor pressures. In the present study, we use isothermal sorption calorimetry, which is suitable for detection of various physicochemical phenomena such as phase transitions and glass transitions. The sorption isotherm of the sample and the corresponding differential enthalpies and entropies of hydration are obtained simultaneously in one experiment.¹⁶ For comparison to initially dry untreated HA, a second sample was prepared where HA was first mixed with water (85 wt % H_2O), equilibrated for several days, and subsequently dried in vacuum and ground in a mortar prior to the sorption experiment. The sorption isotherms and corresponding hydration enthalpy and entropy curves at $25\ ^\circ\text{C}$

$^\circ\text{C}$ are shown in Figure 3. The water content, wt %, is given as the mass of water divided by the total mass of the sample.

As observed from the sorption isotherms in Figure 3a, the untreated material absorbed more water at low water activities compared to the water-pretreated material. This suggests a less ordered state of untreated HA, while the water treatment apparently induced some crystallinity in the material. At higher water activities, the sorption isotherms of untreated and semicrystallized material coincide. In both curves, a clear step in water activity is observed at water contents of approximately 34.0 and 32.5 wt % for the untreated and semicrystallized sample, respectively. Because this event occurs at slightly different water contents, it indicates a nonequilibrium crystallization (marked with the first arrow in Figure 3a). During the following increase in water content, up to approximately 42 wt %, the water activity level is relatively constant, which suggests an equilibrium phase transition between the two arrows in Figure 3a. Above 42 wt % water, the water activity starts to rise again, indicating a one-phase solution. Increased temperature (40 and $50\ ^\circ\text{C}$) shifts these transitions toward lower water content and lower water activity (Supporting Information, Figures S1 and S2).

The corresponding enthalpy and entropy curves are shown in Figure 3b and c, respectively. The two samples show similar events upon hydration, but the events in the pretreated sample are less pronounced. First, a small kink is observed at a water content of about 25 wt %, which suggests a glass transition. At further water sorption, a sharp endothermic peak ($H_w^m > 0$) is observed for the untreated HA sample at a water content of 34 wt % (Figure 3b). Note that this sharp peak coincides with the step (crystallization) observed in the sorption isotherm at 34 wt % water (Figure 3a). The third event, demonstrated as a step in the enthalpy and entropy curves, is consistent with the increase in water activity observed in the sorption isotherm at 42 wt % water. This event is interpreted as dissolution of crystals and is in good agreement with disappearance of optical birefringence upon hydration; see, for example, Figure 2C and D. The entropy curves in Figure 3c show similar profiles as the enthalpy curves, which is explained by the correlation outlined in eq 2. At elevated temperatures, the glass transition and the endothermic phase transition are shifted toward lower water contents (Supporting Information, S3 and S4).

It should also be noted that the enthalpy of hydration at zero water content for untreated HA but not for the semicrystalline

sample is close to -18 kJ/mol . This value has been observed for several other biopolymer systems.^{23–27}

SWAXS. SWAXS was used to determine the structures in HA with respect to the water content at 25 °C. The scattering spectra are shown in Figure 4.

Dry to moderately hydrated HA exists in the amorphous, glassy state. No Bragg reflections were observed for samples with water contents up to 26 wt %, indicating the absence of molecular order. The broad diffuse peak at $q \approx 7.5 \text{ nm}^{-1}$ may comprise contributions from both HA chains in the amorphous state and scattering from individual monosaccharide units.²³ In samples with slightly higher water contents (i.e., 29 and 31 wt %), a second broad peak is observed at $q \approx 3 \text{ nm}^{-1}$. This change in the scattering pattern coincides with the glass transition observed in the enthalpy curve at about 25 wt % water (Figure 3b).

In the low q range ($q < 1 \text{ nm}^{-1}$), the scattering curves for HA with up to 31 wt % water are parallel straight lines with a slope close to -4 . For particle systems with surface fractals, the intensity (I) decays as a function of the scattering vector (q)

$$I = q^{-(6-d_s)} \quad (3)$$

where d_s is the surface fractal dimension.²⁸ Because d_s for a surface fractal in a three-dimensional space can be between 2 and 3, the exponent of q has to be between -3 and -4 , which corresponds to rough and smooth surfaces, respectively. In agreement with the observed slope of -4 , HA particles in the amorphous state have rather smooth surfaces on the nanometer scale ($0.1 < q < 1 \text{ nm}^{-1}$; cf., Figure 2B).

Upon increasing the water content to 34 wt %, a pronounced Bragg peak turns up at $q = 0.21 \text{ nm}^{-1}$ (i.e., $d \approx 30 \text{ nm}$) in the scattering curve, Figure 4a. Several Bragg reflections also appear at higher q values ($\geq 2 \text{ nm}^{-1}$). This is in good agreement with the hydration enthalpy data (Figure 3b) and proves that the endothermic phase transition reflects crystallization. A magnification of this scattering curve on the linear scale ($q = 2\text{--}9 \text{ nm}^{-1}$) is shown in Figure 5 together with an appended WAXS spectra ($q = 13\text{--}19 \text{ nm}^{-1}$).

The HA in the current study was of pharmaceutical grade and used as received without further purification, justified by commercial relevance. However, several authors have reported that HA is prone to crystallize in different polymorphs dependent on the type of cations present and that even traces of multivalent ions may affect the structure.^{11,14,29,30} Nevertheless, assuming pure sodium hyaluronate close to physiological pH, the most probable structure should be based on the orthorhombic unit cell determined by Sheehan et al. with lattice parameters $a = 1.10$, $b = 0.98$, and $c = 3.36 \text{ nm}$ ³⁰ and space group $P2_12_12_1$.¹⁴ Our data do not exclude the proposed structure based on an angular tolerance of $\theta = 0.150^\circ$, but the lattice parameters of the present study deviate slightly from those of Sheehan and co-workers, $a = 1.14$, $b = 1.03$, and $c = 3.13 \text{ nm}$ (Figure 5). Unfortunately, the gap between the X-ray detectors ($q = 9\text{--}13 \text{ nm}^{-1}$, Figure 5) renders data insufficient for a more precise structure determination.

Furthermore, the origin of the Bragg peak at $d = 30 \text{ nm}$ can be verified by using the contour length of the HA polymer and the contraction factor due to crystallization of HA. The estimated contour length ($L_{\text{cont}} = n_{\text{chain}} \cdot l_{\text{ds}}$) of a 17 kDa HA polymer is approximately 42 nm, where n_{chain} is the number of disaccharide units in the chain and l_{ds} is the length of one disaccharide unit ($l_{\text{ds}} = 1 \text{ nm}$ ³¹). The contraction factor is

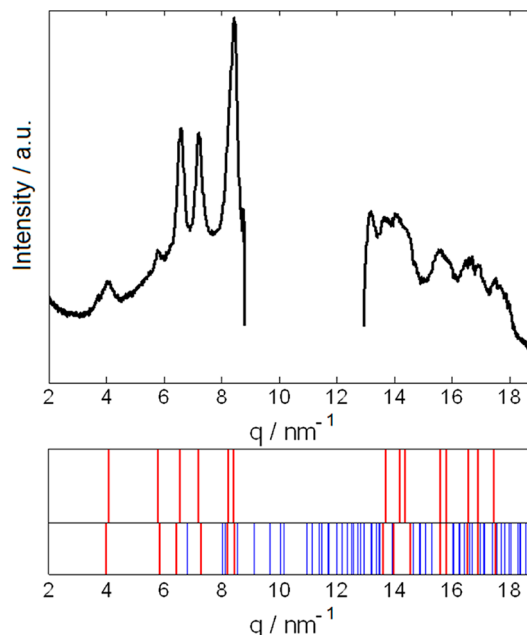


Figure 5. SWAXS spectra of HA hydrated to 34 wt % water. The bar below highlights experimental data (upper part) and theoretical Bragg peaks (lower part) for space group $P2_12_12_1$, $a = 1.14$, $b = 1.03$, and $c = 3.13$. This match is based on an angular tolerance of $\theta = 0.150^\circ$.

defined as the ratio of the polymer end-to-end distance (R_{ee}) in the crystalline state over the contour length, $C_f = R_{\text{ee}}/L_{\text{cont}} = c/(n_{\text{uc}} \cdot l_{\text{ds}})$, where n_{uc} is the number of disaccharide units in one chain within the unit cell. Here, the contraction factor is 0.78, $c/(n_{\text{uc}} \cdot l_{\text{ds}}) = 3.13/4$, and $d = 30 \text{ nm}$ then corresponds to an experimental contour length ($L_{\text{cont}} = d/C_f = 30/0.78$) of 38.5 nm. Because we do not know the exact chain length distribution of the 17 kDa HA polymer, this value is deemed acceptable. Furthermore, at 34 wt % water in the low q range ($q < 1 \text{ nm}^{-1}$), the slope of the linear part of the scattering curve changes from -4 to -3 (Figure 4a), which is indicative of an increase in surface roughness of the HA particles upon crystallization.

At a water content of 50 wt %, the HA crystallites have dissolved to form a gel-like solution. The slope of the scattering curves (50–99 wt % water) in the high q range ($> 4 \text{ nm}^{-1}$) is close to $-5/3$, Figure 4b. The corresponding Flory exponent, ν , ($d_f = 1/\nu$) is close to 0.58 and may reflect self-avoiding swollen chains.³² At very low q ($< 0.2 \text{ nm}^{-1}$), we see a sharp upturn in these scattering curves, which is indicative of long-range concentration fluctuations.³³ Furthermore, in the very dilute regime (99 wt % water), we observe the expected polyelectrolyte peak at $q = 0.6 \text{ nm}^{-1}$, which is in good agreement with previous data presented by Villetti and co-workers.³⁴ Notably, while Villetti et al. had to apply shear to make the peak visible, we observe the peak already when the sample is at rest. One explanation may be the significantly lower molecular weight of HA used in the present study. Absence of this peak in the more condensed samples is probably due to electrostatic screening.

DSC. The thermal behavior of different HA–water samples was studied with DSC. A selection of representative thermograms is shown in Figure 6. The enthalpy of melting of ice was determined for several HA–water samples (Figure 7). From intersection of the straight line with the x -axis, the amount of nonfreezing water per gram of HA was determined to be 0.62

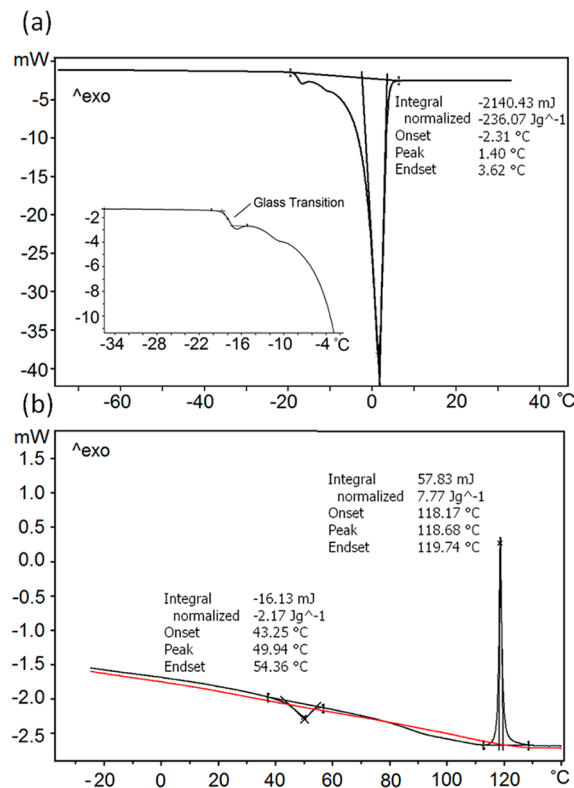


Figure 6. DSC thermograms of two HA samples with (a) 80 and (b) 17 wt % water. Samples with high water content show the glass transition (enlargement (a)), a small endotherm, and the ice melting peak. For samples with low water content, three main events are observed in the first scan (black), the sub- T_g , glass transition, and the exothermic peak, while in the second scan (red), these events are absent.

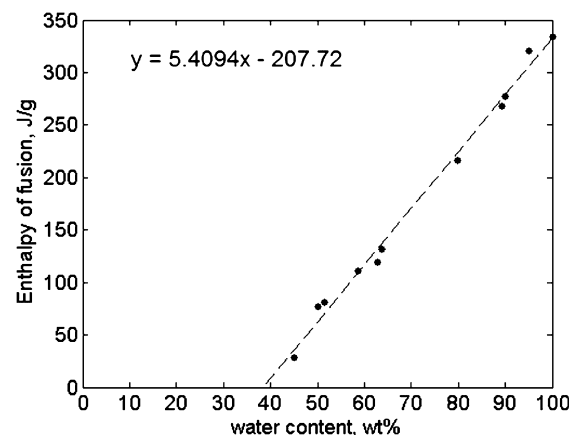


Figure 7. Enthalpy of melting of water (J/g) as a function of water content (wt %) in the HA–water system. The dashed line represents the linear regression used to calculate the amount of nonfreezing water.

g/g. This result is in line with previous studies on HA reporting values between 0.5 and 0.8 g/g of HA.^{20,35,36} In comparison to other biopolymers such as mucin (0.51 g/g),²⁷ acid hydrolyzed starch (0.34 g/g),²³ and native starch (0.36 g/g)²³ HA displays a higher sorption capacity.

In the semidilute to dilute regime (45–96 wt % H₂O), the glass transition temperature (T_g) is independent of water content and occurs at approximately -20 °C; see the example

in the enlargement in Figure 6a. In the same figure, a small endothermic peak is observed after the glass transition, which suggests melting of the crystalline structure in HA.

In contrast to the dilute regime, samples within the concentrated regime (0–35 wt % H₂O) show strong dependence of the T_g on water content, that is, increased water content lowers the T_g . In addition to the glass transition, an endothermic peak and a sharp exothermic peak can be observed in the thermogram for concentrated samples (Figure 6b). In previously reported studies on starch, the endothermic peak appearing prior to the glass transition in the heating curve was referred to as a sub- T_g endotherm.^{23,37} The temperature at which this event occurred decreased with increased water content, while the magnitude of the enthalpy increased with increased water content (Supporting Information, Figures S5 and S6). Much reduced, this event was also observed for dry HA samples, although one cannot completely exclude the presence of traces of water in the sample that is supposed to be dry. In principle, a sub- T_g endotherm can be attributed either to enthalpy relaxation in the glassy state or to polymer–water interactions.³⁷ In the latter case, the effect should not be visible in completely dry samples. Drying of glassy samples is however an experimental challenge due to extremely slow diffusion of water in the glassy state. The exact nature of the sub- T_g endotherm in HA and other biopolymers can be a subject of further investigations.

In more hydrated samples where the glass transition occurs at around -20 °C, the sub- T_g endotherm is not observed. For high polymer concentrations, the sub- T_g event and the glass transition take place at a higher temperature than the equilibration temperature used for hydration (25 °C), meaning that the sample is in a glassy state at room temperature. For more hydrated samples, the temperature at which the sample is equilibrated is above the T_g , and the sample is initially a solution. This may explain why a sub- T_g endotherm is not observed for samples with high water content.

The sharp exothermic peak, which follows after the sub- T_g endotherm and the glass transition, was observed in the first heating scan but not in the second (Figure 6b). This exothermic event is interpreted as crystallization of HA upon heating and will be further discussed in the following section.

Phase Diagram of the HA–Water System. By combining data obtained from several methods, we construct a temperature–composition phase diagram of the HA–water system; see Figure 8. To the best of our knowledge, this is the first phase diagram presented for this system. In what follows, we will discuss some thermodynamic properties related to the hydration- and temperature-induced transitions that are presented in the phase diagram.

As revealed from DSC and sorption calorimetric data, two different regions of glass transitions were observed. At high water content, the glass transition was shown to be independent of hydration level, which in the phase diagram is represented by the horizontal line that separates regions containing glassy and rubbery/flexible HA (Figure 8). In concentrated HA samples on the other hand, water has a strong plasticizing effect, as shown by the clear dependence between the water content and T_g in the phase diagram. Moreover, the difference in heat capacity (ΔC_p) of the glass transition was observed to be higher for dilute samples compared to concentrated samples. For example, ΔC_p (80 wt % water) was determined to be 1.701 J/g·K, and ΔC_p (22.8 wt % water) was found to be 0.150 J/g·K (per mass of the water–polymer

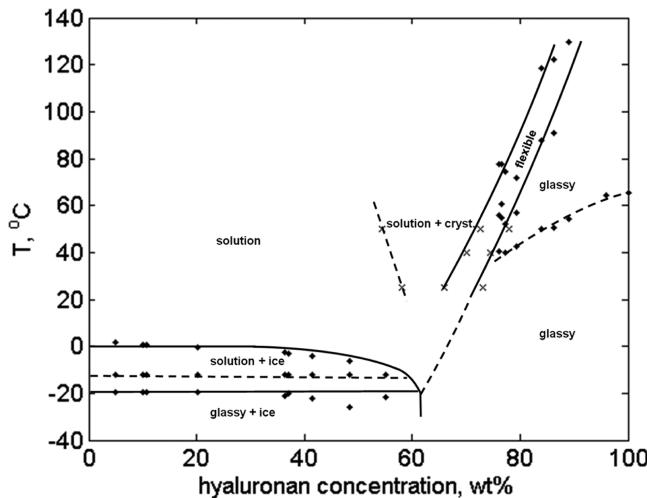


Figure 8. Phase diagram of the HA–water system. (◆) DSC data; (x) sorption calorimetric data. The dashed line to the right side of the phase diagram corresponds to the sub- T_g endotherm. The phase boundary between the flexible polymer and the two-phase region, solution and crystals, is a nonequilibrium transition.

mixture). Apparently, the higher ΔC_p of the glass transition for dilute HA samples is explained by the presence of a two-phase area with contribution not only from the increased mobility of polymer chains but also from the melting of ice.

Above the glass transition, the HA polymer can rearrange, which allows for crystallization, and further addition of water dissolves the crystals to eventually form a one-phase solution (Figure 8). This also results in an intermediate two-phase region with crystals in solution. The phase boundary separating the two-phase region and the solution was determined based on sorption calorimetric data, which suggested a positive slope of the phase boundary with respect to water content. Provided that this phase transition is an equilibrium transition, the van der Waals differential equation for isobaric conditions^{38–40} can be applied to verify the slope dT/dx_w of the phase boundary

$$\left(\frac{dT}{dx_w}\right)^{(1)} = -\frac{RT^2 \left(\frac{d \ln a_w}{(1-x_w)dx_w} \right)^{(1)}_{T,P} \Delta x_w^{1 \rightarrow 2}}{H^{1 \rightarrow 2}} \quad (4)$$

While hydration-induced crystal formation was found to be a nonequilibrium phase transition, melting of crystals is considered to be a reversible phase transition close to equilibrium conditions. We will therefore in this case discuss the crystallization by going from left to right in the phase diagram (Figure 8). As previously shown,^{38,41} the enthalpy term $H^{1 \rightarrow 2}$ in eq 4 can be obtained from the integral of the hydration enthalpy if the baseline is taken from the first phase

$$H^{1 \rightarrow 2} = (1 - x_w^{(2)}) \int_{r(1)}^{r(2)} (H_w^m - H_w^{m(1)}) dr \quad (5)$$

where r denotes the water to polymer mole ratio in phase (1) or (2) and $x_w^{(2)}$ denotes the mole fraction of water in phase (2). $H_w^{m(1)}$ and H_w^m correspond to the hydration enthalpy before the transition and during the transition, respectively. If we define phase (1) as the solution phase, then it is shown in Figure 3b that the enthalpy level of the solution H_w^m (above 42 wt % water) is higher compared to the enthalpy level at the phase transition $H_w^{m(1)}$ (at 42 wt % water). Because $r^{(1)}$ is higher than $r^{(2)}$

in this case, the integral in eq 5 is positive, which results in a positive enthalpy term $H^{1 \rightarrow 2}$, and the phase transition is endothermic. Taken together, we may therefore conclude that an endothermic phase transition ($H^{1 \rightarrow 2} > 0$) should result in a positive slope $dT/dx_w^{(1)}$ according to the van der Waals differential equation (eq 4). Thus, the unusual sign of the enthalpy of the crystallization transition observed in sorption calorimetry is consistent with the slope of the phase boundary in the phase diagram.

We will now focus on the nonequilibrium crystallization of HA. From the enthalpy curve in Figure 3b, one can see that formation of HA crystals upon hydration is manifested as a sharp endothermic peak ($H_w^m > 0$). However, at lower water contents and higher temperatures, the heat effect of HA crystallization was shown to be negative (exothermic) in the DSC scans; see the example in Figure 6b. The molecular-level explanation to this experimental fact can be based on the hydrophobic effect in the HA–water system. As known, water molecules around small hydrophobic solutes can preserve all four hydrogen bonds, while for sufficiently large hydrophobic clusters, all hydrogen bonds cannot circumvent the hydrophobic region.⁴² Some of the hydrogen bonds near the large hydrophobic cluster must thus be broken. Similar reasoning can be applied to the HA–water system. For a single HA polymer chain, the adjacent water molecules may maintain a complete hydrogen-bonding network. However, for HA helices formed in a crystalline state, the situation will be different. Due to the topology of the crystalline structure, the hydrophobic domain becomes continuous and larger compared to the ones in a single chain. Some of the water–water hydrogen bonds may thus be lost near the hydrophobic domains, which is in agreement with the endothermic heat effect of crystallization shown in Figure 3b. Furthermore, as HA chains aggregate into a crystalline structure, water molecules that surrounded hydrophobic domains of the free chains can be released, which contributes to a positive value of the partial molar entropy of mixing of water S_w^m , as seen in Figure 3c. The formation of crystalline structure at high water content is therefore driven by entropy.

However, crystallization at lower water contents and higher temperatures turned out to be exothermic; see the example in the DSC scan in Figure 6b. Here, the amount of water is insufficient for considering the polymer chains to be fully hydrated and surrounded by the three-dimensional network of liquid water, required for the hydrophobic effect. Crystal formation occurs due to interactions between hydrophobic domains and formation of more directed and therefore stronger hydrogen bonds within and between HA helices of the crystalline structure. In the latter case, crystallization is driven by enthalpy. It should though be noted that the two mechanisms, which determine the sign of the heat effect of crystallization, may coexist. This is illustrated in Figure 9, which shows a gradual change in crystallization enthalpy as a function of water content.

The mechanisms of solubility of carbohydrate polymers are currently under debate; in particular, the role of hydrophobic interactions versus hydrogen bonding is discussed.^{43,44} The results reported here may be of interest in this discussion because they indicate that both hydrogen bonding and the hydrophobic effect influence the crystallization process, but their relative contributions depend on experimental conditions.

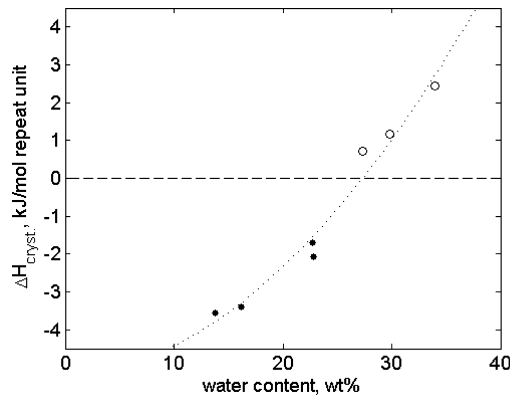


Figure 9. Enthalpy of the nonequilibrium crystallization transition as a function of water content in the HA–water system. The open circles correspond to data obtained by sorption calorimetry, and the solid circles correspond to data obtained by DSC.

4. CONCLUSIONS

We have used isothermal sorption calorimetry, differential scanning calorimetry, synchrotron radiation X-ray scattering, and light and scanning electron microscopy to examine the structure and thermodynamic properties of sodium hyaluronate (HA, 17 kDa) with respect to hydration and temperature. Our findings are used to construct a binary phase diagram of the HA–water system, and the main conclusions are as follows:

- The dry HA is initially in the amorphous glassy state.
- Upon hydration at 25 °C, HA demonstrates a glass transition at 25 wt % water followed by a crystallization at 34 wt % water and finally dissolution of crystals, which results in a one-phase solution above 42 wt % water.
- The phase diagram reflects two different regions comprising a glass transition, one in which the transition is dependent on the water content and one in which it is independent. In moderately hydrated HA samples (up to 35 wt % H₂O), water has a strong plasticizing effect on the T_g of HA, while for dilute samples (from 45 wt % H₂O), T_g was found to be close to -20 °C.
- X-ray data confirm crystallization of HA upon hydration. Structural analysis reveals that the crystal may be indexed on an orthorhombic unit cell with lattice parameters $a = 1.14$, $b = 1.03$, and $c = 3.13$ nm and space group $P2_12_12_1$.
- Crystallization of HA at higher water contents is endothermic and is driven by entropy due to the hydrophobic effect, while at lower water contents and higher temperatures, crystallization is exothermic.
- The amount of nonfreezing water in HA was determined to be 0.62 g/g. This value is higher than that obtained for other biopolymers, such as mucin (0.51 g/g) and starch (0.36 g/g).

■ ASSOCIATED CONTENT

Supporting Information

Additional figures showing the sorption isotherm and hydration enthalpy of HA at 40 and 50 °C as well as the relation between temperature and enthalpy of a sub- T_g endotherm versus water content. This material is available free of charge via the Internet at <http://pubs.acs.org>.

■ AUTHOR INFORMATION

Corresponding Author

*E-mail: vitaly.kocherbitov@mah.se. Tel: +46-66 57946. Address: Department of Biomedical Science, Malmö University, SE-205 06 Malmö, Sweden.

Notes

The authors declare no competing financial interest.
E-mail: cathrine.alber@mah.se (C.A.). johan.engblom@mah.se (J.E.). peter.falkman@mah.se (P.F.).

■ ACKNOWLEDGMENTS

We would like to thank Katarina Edsman (Q-Med AB), Ulrika Sandkvist (Q-Med AB), Jonas Carlstedt (Malmö University), Robert Corkery (KTH), Marie Lodén (Eviderm Institute AB), and Ulf Åkerström (ACO Hud AB) for valuable discussions. MAX IV Laboratory is gratefully acknowledged for giving us the opportunity to perform SAXS experiments, and we are especially grateful to Tomàs S. Plivelic and Sylvio Haas for technical assistance. Financial support from the Knowledge Foundation (Stiftelsen för kunskaps- och kompetensutveckling, Sweden), Gustav Th Ohlsson Foundation (Sweden), and Malmö University (Sweden) is gratefully acknowledged.

■ REFERENCES

- (1) Balazs, E. A.; Laurent, T. C.; Jeanloz, R. W. Nomenclature of Hyaluronic-Acid. *Biochem. J.* **1986**, *235*, 903–903.
- (2) Fraser, J. R. E.; Laurent, T. C.; Laurent, U. B. G. Hyaluronan: Its Nature, Distribution, Functions and Turnover. *J. Int. Med.* **1997**, *242*, 27–33.
- (3) Cowman, M. K.; Matsuoka, S. Experimental Approaches to Hyaluronan Structure. *Carbohydr. Res.* **2005**, *340*, 791–809.
- (4) Miller, D.; Stegmann, R. The Use of Healon in Intraocular Lens Implantation. *Int. Ophthalmol. Clin.* **1982**, *22*, 177–87.
- (5) Miller, D.; Stegmann, R. *Healon (Sodium Hyaluronate). A Guide to Its Use in Ophthalmic Surgery*; Wiley: New York, 1983.
- (6) Price, R. D.; Berry, M. G.; Navsaria, H. A. Hyaluronic Acid: The Scientific and Clinical Evidence. *J. Plast. Reconstr. Aesthet. Surg.* **2007**, *60*, 1110–1119.
- (7) Stern, R. Hyaluronan: Key to Skin Moisture. In *Dry Skin and Moisturizers*, 2nd ed.; Lodén, M., Maibach, H. I., Eds.; Taylor & Francis Group: Boca Raton, FL, 2006; pp 245–278.
- (8) Hayashi, K.; Tsutsumi, K.; Nakajima, F.; Norisuye, T.; Teramoto, A. Chain Stiffness and Excluded Volume Effects in Solutions of Sodium Hyaluronate at High Ionic Strength. *Macromolecules* **1995**, *28*, 3824–3830.
- (9) Scott, J. E.; Cummings, C.; Brass, A.; Chen, Y. Secondary and Tertiary Structures of Hyaluronan in Aqueous Solutions, Investigated by Rotary Shadowing Electron Microscopy and Computer Simulation. Hyaluronan Is a Very Efficient Network Forming Polymer. *Biochem. J.* **1991**, *274*, 699–705.
- (10) Scott, J. E.; Heatley, F. Hyaluronan Forms Specific Stable Tertiary Structures in Aqueous Solution: A ¹³C NMR Study. *Proc. Natl. Acad. Sci. U.S.A.* **1999**, *96*, 4850–4855.
- (11) Arnott, S.; Mitra, A. K.; Raghunathan, S. Hyaluronic-Acid Double Helix. *J. Mol. Biol.* **1983**, *169*, 861–872.
- (12) Atkins, E. D. T.; Sheehan, J. K. Hyaluronates — Relation between Molecular Conformations. *Science* **1973**, *179* (4073), 562–564.
- (13) Mitra, A. K.; Arnott, S.; Sheehan, J. K. Hyaluronic Acid — Molecular Conformation and Interactions in the Tetragonal Form of the Potassium Salt Containing Extended Chains. *J. Mol. Biol.* **1983**, *169*, 813–827.
- (14) Mitra, A. K.; Raghunathan, S.; Sheehan, J. K.; Arnott, S. Hyaluronic Acid — Molecular Conformations and Interactions in the Orthorhombic and Tetragonal Forms Containing Sinuous Chains. *J. Mol. Biol.* **1983**, *169*, 829–859.

- (15) Greenspan, L. Humidity Fixed-Points of Binary Saturated Aqueous Solutions. *J. Res. Natl. Bur. Stand., Sect. A* **1977**, *81*, 89–96.
- (16) Wadso, L.; Markova, N. A Method to Simultaneously Determine Sorption Isotherms and Sorption Enthalpies with a Double Twin Microcalorimeter. *Rev. Sci. Instrum.* **2002**, *73*, 2743–2754.
- (17) Kocherbitov, V. A New Formula for Accurate Calculation of Water Activity in Sorption Calorimetric Experiments. *Thermochim. Acta* **2004**, *414*, 43–45.
- (18) Labrador, A.; Cerenius, Y.; Svensson, C.; Theodor, K.; Plivelic, T., The Yellow Mini-Hutch for SAXS Experiments at Max IV Laboratory. 11th International Conference on Synchrotron Radiation Instrumentation (SRI 2012), Lyon, France, July 9–13, 2012; 2013; p 425.
- (19) Block, A.; Bettelheim. Water Vapor Sorption of Hyaluronic Acid. *Biochim. Biophys. Acta* **1970**, *201* (1), 69.
- (20) Jouon, N.; Rinaudo, M.; Milas, M.; Desbrieres, J. Hydration of Hyaluronic Acid as a Function of the Counterion Type and Relative Humidity. *Carbohydr. Polym.* **1995**, *26*, 69–73.
- (21) Panagopoulou, A.; Molina, J. V.; Kyritsis, A.; Pradas, M. M.; Lluch, A. V.; Ferrer, G. G.; Pissis, P. Glass Transition and Water Dynamics in Hyaluronic Acid Hydrogels. *Food Biophys.* **2013**, *8*, 192–202.
- (22) Servaty, R.; Schiller, J.; Binder, H.; Arnold, K. Hydration of Polymeric Components of Cartilage — An Infrared Spectroscopic Study on Hyaluronic Acid and Chondroitin Sulfate. *Int. J. Biol. Macromol.* **2001**, *28*, 121–127.
- (23) Carlstedt, J.; Wojtasz, J.; Fyhr, P.; Kocherbitov, V. Hydration and the Phase Diagram of Acid Hydrolyzed Potato Starch. *Carbohydr. Polym.* **2014**, *112*, 569–77.
- (24) Kocherbitov, V.; Arnebrant, T.; Soderman, O. Lysozyme–Water Interactions Studied by Sorption Calorimetry. *J. Phys. Chem. B* **2004**, *108*, 19036–19042.
- (25) Kocherbitov, V.; Ulvenlund, S.; Briggner, L. E.; Kober, M.; Arnebrant, T. Hydration of a Natural Polyelectrolyte Xanthan Gum: Comparison with Non-Ionic Carbohydrates. *Carbohydr. Polym.* **2010**, *82*, 284–290.
- (26) Kocherbitov, V.; Ulvenlund, S.; Kober, M.; Jarring, K.; Arnebrant, T. Hydration of Microcrystalline Cellulose and Milled Cellulose Studied by Sorption Calorimetry. *J. Phys. Chem. B* **2008**, *112*, 3728–3734.
- (27) Znamenskaya, Y.; Sotres, J.; Engblom, J.; Arnebrant, T.; Kocherbitov, V. Effect of Hydration on Structural and Thermodynamic Properties of Pig Gastric and Bovine Submaxillary Gland Mucins. *J. Phys. Chem. B* **2012**, *116*, 5047–5055.
- (28) Roe, R.-J. *Methods of X-Ray and Neutron Scattering in Polymer Science*; Oxford University Press, Inc.: New York, 2000.
- (29) Hargittai, I.; Hargittai, M. Molecular Structure of Hyaluronan: An Introduction. *Struct. Chem.* **2008**, *19*, 697–717.
- (30) Sheehan, J. K.; Atkins, E. D. T. X-ray Fiber Diffraction Study of Conformational Changes in Hyaluronate Induced in the Presence of Sodium, Potassium and Calcium Cations. *Int. J. Biol. Macromol.* **1983**, *5*, 215–221.
- (31) Cowman, M. K.; Masuoka, S. The Intrinsic Viscosity of Hyaluronan. In *Hyaluronan — Chemical, Biochemical and Biological Aspects*; Kennedy, J. F., Philips, G. O., Williams, P. A., Hascall, V. C., Eds.; Woodhead Publishing Ltd: Cambridge, England, 2002; Vol. 1, p 78.
- (32) Muthukumar, M. *Polymer Translocation*; CRC Press, Taylor & Francis Group: Boca Raton, FL, 2011.
- (33) Ermi, B. D.; Amis, E. J. Domain Structures in Low Ionic Strength Polyelectrolyte Solutions. *Macromolecules* **1998**, *31*, 7378–7384.
- (34) Villetti, M.; Borsali, R.; Diat, O.; Soldi, V.; Fukada, K. SAXS from Polyelectrolyte Solutions under Shear: Xanthan and Na-Hyaluronate Examples. *Macromolecules* **2000**, *33*, 9418–9422.
- (35) Yoshida, H.; Hatakeyama, T.; Hatakeyama, H. Characterization of Water in Polysaccharide Hydrogels by DSC. *J. Therm. Anal.* **1993**, *40*, 483–489.
- (36) Prusova, A.; Smejkalova, D.; Chytil, M.; Velebny, V.; Kucerik, J. An Alternative DSC Approach to Study Hydration of Hyaluronan. *Carbohydr. Polym.* **2010**, *82*, 498–503.
- (37) Thiewes, H. J.; Steeneken, P. A. M. The Glass Transition and the Sub- T_g Endotherm of Amorphous and Native Potato Starch at Low Moisture Content. *Carbohydr. Polym.* **1997**, *32*, 123–130.
- (38) Kocherbitov, V. Application of Scanning Methods to Distinguish between Entropy and Enthalpy Driven Phase Transitions. *Curr. Opin. Colloid Interface Sci.* **2013**, *18*, 510–516.
- (39) Storonkin, A. *Termodynamika Geterogennykh Sistem*; Izd-vo Leningradskogo Un-ta: Leningrad, Russia, 1967; Vol. 2.
- (40) Waals, J.; Kohnstamm, P. *Lehrbuch Der Thermostatis. Das Heisst Des Thermischen Gleichgewichtes Materieller Systeme*; Johann Ambrosius Barth: Leipzig, Germany, 1927.
- (41) Kocherbitov, V. Salt-Saturated Salt Solution as a Standard System for Sorption Calorimetry. *Thermochim. Acta* **2004**, *421* (1–2), 105–110.
- (42) Chandler, D. Interfaces and the Driving Force of Hydrophobic Assembly. *Nature* **2005**, *437* (7059), 640–647.
- (43) Glasser, W. G.; Atalla, R. H.; Blackwell, J.; Brown, R. M., Jr.; Burchard, W.; French, A. D.; Klemm, D. O.; Nishiyama, Y. About the Structure of Cellulose: Debating the Lindman Hypothesis. *Cellulose* **2012**, *19*, 589–598.
- (44) Medronho, B.; Romano, A.; Miguel, M. G.; Stigsson, L.; Lindman, B. Rationalizing Cellulose (In)Solubility: Reviewing Basic Physicochemical Aspects and Role of Hydrophobic Interactions. *Cellulose* **2012**, *19*, 581–587.